Temporal multi-omics identifies LRG1 as a vascular niche instructor of metastatic colonization

Mahak Singhal[1,2,3,#,*], Nicolas Gengenbacher[1,2,3,#], Ashik Ahmed Abdul Pari[1,2,3,#], Miki Kamiyama[1,2], Ling Hai[4], Bianca Kuhn[3,5], David M. Kallenberg[6], Eva Besemfelder[1], Barbara Leuchs[7], Carolin Mogler[8], Jeroen Krijgsveld[5], Matthias Schlesner[4], Junhao Hu[9], Stephen E. Moss[6], John Greenwood[6], Hellmut G. Augustin[1,2,10,*]

[1]Division of Vascular Oncology and Metastasis, German Cancer Research Center (DKFZ-ZMBH Alliance), Heidelberg, Germany. [2]Department of Vascular Biology and Tumor Angiogenesis, European Center for Angioscience (ECAS), Medical Faculty Mannheim, Heidelberg University, Mannheim, Germany. [3]Faculty of Biosciences, Heidelberg University, Germany. [4]Junior Group Bioinformatics and Omics Data Analytics, German Cancer Research Center (DKFZ), Heidelberg, Germany. [5]Divison of Proteomics of Stem Cells and Cancer, German Cancer Research Center (DKFZ), Heidelberg, Germany. [6]Department of Cell Biology, UCL Institute of Ophthalmology, London, United Kingdom. [7]Vector Development & Production Unit, German Cancer Research Center (DKFZ), Heidelberg, Germany. [8]Institute of Pathology, TUM School of Medicine, Munich, Germany. [9]Interdisciplinary Research Center on Biology and Chemistry, Shanghai Institute of Organic Chemistry, Chinese Academy of Sciences, Shanghai, China. [10]German Cancer Consortium, Heidelberg, Germany.

[#]equally contributing first authors; [*]Corresponding authors

One sentence summary: A systems-biology endothelial cell screen has established the vascular systems map of early metastatic colonization and identified the TGFβ pathway specifier as therapeutic target of metastasis.

Short title: LRG1 facilitates metastatic colonization

Keywords: metastasis, vascular niche, angiocrine factors

Word count: 2,190

Word count abstract: 208

Address correspondence to:
Dr. Hellmut G. Augustin
European Center for Angioscience (ECAS), Medical Faculty Mannheim, Heidelberg University,
and German Cancer Research Center (DKFZ-ZMBH Alliance)
Im Neuenheimer Feld 280, 69120 Heidelberg, Germany
Phone: +49-6221-421500
Fax: +49-6221-421515
Email: augustin@angiogenese.de

Metastasis is the primary cause of cancer-related mortality and the mechanistically least well understood step of the tumour progression cascade[1-3]. Tumour cell interactions with cells of the vessel wall are decisive and rate-limiting for metastasis[4-6]. The past decade has witnessed a fundamental change of paradigm from blood vessel wall-lining endothelial cells (EC) being conceived as merely supportive of angiogenesis to an active gatekeeper and modulator of the tumour microenvironment[7-12]. The molecular nature of this crosstalk is beyond candidate gene approaches hitherto poorly understood. Employing surgical models of lung metastasis in temporal systems biology-based screens, we show here that primary tumours systemically reprogram the body's vascular endothelium to perturb homeostasis and to precondition the vascular niche for metastatic colonization. The vasculature with its enormous surface thereby serves as amplifier of tumour-induced instructive signals. The combined endothelial transcriptomic and serum proteomic screen identified the TGFβ pathway signalling specifier LRG1 as an early instructor of metastatic colonization. Systemic upregulation of LRG1 promoted metastasis by increasing the number of prometastatic NG2+ perivascular cells. In turn, adjuvant LRG1 inhibition in primary tumour-resected mice delayed metastatic growth and increased overall survival. The study has thereby established the systems map of early primary tumour-induced vascular changes and identified LRG1 as a therapeutic target for metastasis.

In order to identify molecular changes of EC in the premetastatic and metastatic niche in an unbiased systems biology approach, we employed surgical metastasis models[13] and transcriptionally profiled target organ EC over time. A primary screen was performed by subcutaneously inoculating lung metastasising tumour cells (Lewis Lung Carcinoma, LLC) in C57BL/6N mice and analysing lung EC at sequential stages of tumour progression, including control (d0), small primary tumour-bearing (d15), 1 wk post-primary tumour resection (d22), and metastasis-bearing (d36) (Fig. 1a). Lung EC were isolated in high purity and used for global transcriptomic profiling (Extended Data Fig. 1a-c). Differential gene expression analysis revealed transcriptional activation of EC upon disease progression (Fig. 1b-d, Extended Data Fig. 1d). Most-significantly altered genes at d15 and d36 were related to protein secretion, inflammatory responses, hypoxia, and cellular proliferation (Fig. 1e, Extended Data Fig. 2a). The presence of a primary tumour evoked a systemic inflammation[14,15], as evidenced by an inflammatory transcriptomic signature of lung EC (Fig. 1f, g). Concomitantly, a strong immune cell infiltration, particularly of myeloid cells, was observed in d15 lung tissue as compared to d0 (Fig. 1h, Extended Data Fig. 2b, 3a-d). A sharp decline in the expression of inflammatory genes and corresponding infiltrating immune cells was observed at d22 (Fig. 1h, Extended Data Fig. 2a, b, 3a-d), suggesting subsided systemic inflammation following primary tumour resection. Hence, the employed metastasis model truthfully captured the tumour cell-driven systemic alterations including initial myelopoiesis during primary tumour growth, rapid restoration of homeostasis following tumour resection, and finally myeloid cell expansion upon metastatic colonization. Surprisingly though, the immune cell infiltration in d36 lung tissue was mostly restricted to the adjacent normal tissue rather than the metastatic nodules (Fig. 1h, Extended Data Fig. 2b). Taken together, the data emphasize that the vascular and

immune compartments within a metastatic organ exhibited a defined temporal signature that mirrors the kinetics of disease progression. Further comparative gene ontology analyses of disease and bio-functions not only supported the immune-phenotyping data but additionally identified disease stage-specific regulation of neovascularization-, cell viability- and metastasis-related gene sets (Fig. 2a).

Zooming-in on genes involved in EC development bio-function, *Lrg1* was identified as one of the most differentially expressed EC-specific genes (Fig. 2b, c, Extended Data Fig. 4a). *Lrg1* expression closely reflected the temporal pattern of systemic inflammation, thereby classifying *Lrg1* as an immediate endothelial response gene to tumour challenge. LRG1, Leucine-rich alpha-2-glycoprotein 1, was reported to modulate endothelial TGFβ-signalling[16]. Mechanistically, in the presence of TGFβ1, LRG1 interacts with the accessory receptor Endoglin, thereby switching the EC phenotype from quiescence-mediating ALK5 signalling to activation-inducing ALK1 signalling[16]. Indeed, upstream regulator analysis of the RNA-seq data revealed TGFβ as a positively-correlated signalling effector as well as the enrichment of subsequent downstream signalling cascades during metastatic progression (Extended Data Fig. 5a-c). Altered TGFβ-signalling and overall activation of lung endothelium suggested a counter-regulation of the recently described vascular maturation program[17].

Endothelial STAT3 signalling has been described to actively orchestrate EC responses to inflammation and during metastasis[11,18,19]. Concurrently, we found STAT3 signalling enriched in a disease stage-specific manner in lung EC (Fig. 2d, Extended Data Fig. 2a). To investigate whether STAT3 transcriptionally regulates *Lrg1* expression, we employed EC-specific genetic deletion of *Stat3* (Extended Data Fig. 6a). Indeed, *Stat3* deletion strongly abrogated *Lrg1* expression in lung EC isolated from tumour-bearing mice (Fig. 2e). Further, primary tumour experiments in immunocompromised NSG mice manifested reduced levels of *Lrg1* as compared to immunocompetent C57BL/6N mice (Extended Data Fig. 6b). Additionally, tumour cell-derived factors failed to directly induce *Lrg1* expression in mouse lung EC in *in vitro* Boyden chamber-based experiments (Extended Data Fig. 6c), thereby establishing LRG1 as an endothelial-response factor to tumour-induced systemic inflammation, but not directly tumour cell-derived factors.

We next performed proteomic analyses of serum specimens at sequential stages of LLC tumour progression. Consistent with the transcriptomic screen, LRG1 was one of the most abundant proteins differentially upregulated in d15 serum as compared to d0 specimens (Fig. 2f). Supporting the lung EC bulk RNA-seq data, the serum levels of circulating LRG1 closely reflected the temporal pattern of disease progression (Fig. 2g, Extended Data Fig. 7a).

To confirm the findings of the LLC screen in a second, less reductionist tumour model, we orthotopically implanted small bio-banked MMTV-PyMT breast tumour fragments in the mammary fat pads of syngeneic FVB/N mice (Extended Data Fig. 8a), and traced spontaneous metastasis. Similar to the LLC model, *Lrg1* was upregulated in lung EC and in serum during metastatic progression in the MMTV-PyMT model (Extended Data Fig. 8b, c). Correspondingly, a meta-analysis of several retrospective clinical studies[20-24] revealed an upregulation of serum

LRG1 levels for different human cancer entities as compared to corresponding cohorts of healthy volunteers, including colorectal, gastric, lung, ovarian, and pancreatic tumours (Fig. 2h). These data underline the systemic regulation of LRG1 during metastatic progression.

To determine the primary source of circulating LRG1, we compared *Lrg1* expression amongst *in vitro*-cultured LLC cells, primary tumours, and d15 lung tissue. While LLC cells did not express *Lrg1*, small levels of *Lrg1* were detectable in the primary tumour (Fig. 3a). Notably however, lung tissue displayed substantially stronger *Lrg1* expression as primary tumour tissue (Fig. 3a). To further dissect the cellular source of *Lrg1*, we isolated EC, leukocytes, and $CD31^{-}CD45^{-}$ cells from both, primary tumour and lung tissue. *Lrg1* expression was enriched in the EC population (Fig. 3b, Extended Data Fig. 9a). Nevertheless, infiltrating leukocytes did express detectable levels of *Lrg1* in primary tumours (Fig. 3b). Next, to investigate the role of leukocyte-derived LRG1 in tumour progression, bone marrow (BM) chimeric mice were generated with either WT or *Lrg1*-KO BM cells (Extended Data Fig. 9b-d). Lack of leukocyte-derived LRG1 neither affected primary tumour vasculature (Extended Data Fig. 9e, f), nor did it impact overall survival of mice when compared to the WT BM-chimeras (Fig. 3c). Taken together, EC appear to represent the major cellular source of LRG1, and leukocyte-derived LRG1 is largely-dispensable during metastasis.

To gain insights into EC transcriptomic heterogeneity and to map *Lrg1* expression across EC subpopulations, we conducted single-cell RNA sequencing of lung EC isolated at sequential stages of tumour progression. The cellular heterogeneity was investigated both, within and between the samples by applying uniform manifold approximation and projection (UMAP) and graph-based clustering. Following biologically-supervised filtering (Extended Data Fig. 10a), 8,512 cells were annotated as capillary (sub-cluster I/II), arterial, venous, and cycling populations based on the top 10 differentially-expressed genes in each cluster (Fig. 3d, e). The cluster annotation was in line with the current knowledge of prominent EC signalling families including Vegf-Vegfr, Ang-Tie, and Notch (Extended Data Fig. 10b), and corroborated with recently published single-cell data of homeostatic brain and lung EC[25]. Unexpectedly, the clustering of lung EC remained unaffected during metastasis progression (Extended Data Fig. 10c). Additionally, there were no overt changes in the distribution of cells amongst the clusters (Extended Data Fig. 10d), thereby negating any major restructuring of the vascular hierarchical network as metastatic disease progressed.

Approximately 60% of venous EC were found positive for *Lrg1* expression (Fig. 3f), attributing to the fact that LRG1 was initially identified as a marker for high-endothelial venules[26]. Yet, $Lrg1^{+}$ venous cells constituted merely 20% of total $Lrg1^{+}$ cells, while the remaining 80% of $Lrg1^{+}$ cells were uniformly dispersed amongst the other EC clusters (Fig. 3g). Whilst the frequency of cells expressing *Lrg1* (Log_2-normalized expression >0) remained largely unchanged between the samples, d15 and d36 witnessed a much higher fraction of total cells with elevated levels of *Lrg1* expression (Fig. 3h). In concordance with the bulk RNA-seq data, the single-cell data highlighted a systemic upregulation of *Lrg1* expression throughout all lung EC in a tumour stage-specific pattern. Additionally, we examined *Lrg1* expression levels in different organ EC and found them to be strongly upregulated at d15 across all examined

vascular beds when compared to the resting vasculature (Fig. 3i). The multiorgan increase in *Lrg1* expression was reversed by EC-specific deletion of *Stat3* (Fig. 3j), highlighting STAT3 as a key transcriptional regulator of systemic EC *Lrg1* expression. It is noteworthy that enhanced *Lrg1* expression across multiple vascular beds might have resulted in the observed increase in serum levels of LRG1, thereby indicating that a primary tumour utilizes the large surface of the body's vascular endothelium as an amplifier of tumour-induced systemically acting angiocrine signals.

To dissect the function of LRG1 during metastatic progression, we established a systemic gain-of-function (GOF) experiment by ectopically expressing *Lrg1* in LLC cells (Extended Data Fig. 11a-c). Mice were subcutaneously implanted with LLC-pLenti or LLC-Lrg1 tumours. Upon attaining an average tumour size of just 50 mm^3, they were intravenously injected with melanoma (B16F10) cells (Extended Data Fig. 11d). Mice with systemic upregulation of LRG1 exhibited a strong increase in melanoma lung metastases (Fig. 4a), thereby establishing a pro-metastatic role of systemic LRG1. Likewise, in an experimental liver metastasis model, intravenous injection of WT31 cells resulted in a higher metastatic incidence in mice with systemic GOF of LRG1 (Extended Data Fig. 11e, f). To further decipher the exact step of the metastatic cascade, LLC-pLenti and LLC-Lrg1 tumours were resected 24 h after intravenous injection of B16F10 cells (Extended Data Fig. 12a). There were no differences observed between the two groups suggesting that the pro-metastatic effect of systemic LRG1 was rapidly lost upon withdrawal of the source of LRG1 during metastatic colonization (Extended Data Fig. 12b). To conclusively rule any possible direct effect of LRG1 on tumour cell extravasation, mice were preconditioned with a single injection of either LRG1-neutralizing antibody (anti-LRG1) or control-IgG prior to intravenous injection of melanoma cells (Extended Data Fig. 12c). Consistent with the previous results, blocking LRG1 did not affect the extravasation of melanoma cells (Extended Data Fig. 12d). Collectively, systemically elevated levels of LRG1 supported colonization of disseminated tumour cells.

To investigate the functional impact of LRG1 on the metastatic niche, we quantitated different stromal populations in the lung (Extended Data Fig. 13a). Surprisingly, LRG1 neither influenced EC proliferation nor did it affect the infiltration of different immune cells (Fig. 4b, Extended Data Fig. 13b-d), thereby indicating an angiogenesis- and immune-independent role LRG1 during metastasis. Intriguingly, we observed a strong increase in lung perivascular cells with systemic upregulation of LRG1 (Fig. 4c-e). These NG2+ perivascular cells were recently described to establish a conducive metastatic niche and facilitate metastasis[27]. Therefore, the data suggest that EC-derived LRG1 activates perivascular cells to support metastatic colonization.

Lastly, to assess the therapeutic potential of the LRG1-neutralizing antibody 15C4[28] in clinically relevant settings, we adopted two therapeutic strategies – short-term perioperative and long-term postsurgical adjuvant therapy (Fig. 4f). Perioperative therapy was initiated after LLC tumours had grown to an average size of 150 mm^3 and therapy was discontinued 10 days post-primary tumour resection. This short-term treatment had no apparent effect on the primary tumour vasculature (Extended Data Fig. 14a). Yet, perioperative therapy with anti-LRG1

yielded a significant overall survival advantage (Fig. 4g). To circumvent any effect on primary tumour growth or early steps in the metastatic cascade such as intravasation and extravasation, we next employed an adjuvant therapy approach wherein administration of anti-LRG1 or control-IgG was commenced 1-day post-primary tumour resection until the experimental endpoint. Similar to the perioperative approach, long-term adjuvant therapy prolonged overall survival of mice by 8.5 days, which corresponded to an approximately 40% improvement over the control-IgG treated group (Fig. 4h). Remarkably, anti-LRG1 as a monotherapy offered a substantial overall survival advantage in a mouse model which has previously been reported to be refractory to anti-VEGF therapy[29] and in which chemotherapy shows no effect on lung metastatic burden[11]. Overall, neutralizing LRG1 suppressed tumour cell colonization, thereby providing a significant survival benefit in a clinically-relevant therapeutic window.

In summary, exploiting a comparative systems biology approach, the present study captured the temporal evolution of vascular changes in the pre-metastatic and metastatic niches. In-depth bulk RNA-seq analysis of lung EC complemented with serum proteomics served as a versatile tool for the identification of novel angiocrine molecules. Furthermore, transcriptomics at single-cell resolution mapped endothelial heterogeneity and spatial expression of angiocrine instructors in a tumour cell-seeded lung. The single-cell data added another layer of complexity by attributing spatial information, especially about the arterio-venous axis, which would be diluted in bulk RNA-seq analysis. Notably, the high-resolution expression analysis identifying widespread regulation of LRG1 expression throughout the vascular tree supports the notion that the vascular endothelium serves as an amplifier of tumour-induced systemically-acting instructive signals.

The temporal approach with surgical removal of the primary tumour facilitated for the first time to formally discriminate between pre-metastatic and metastatic EC transcriptomic changes. We prototypically datamined for secreted angiocrine factors and identified the TGFβ pathway specifier LRG1 as an early EC-specific STAT3-dependent responsive signal that was tightly calibrated to the tumour-induced inflammation. Systemic upregulation of LRG1 was dispensable for extravasation but facilitated early-stage colonization of tumour cells at distant metastatic sites. Concomitantly, intervention with anti-LRG1 suppressed metastatic progression in a clinically-relevant adjuvant regimen. Recently, a phase I/IIa clinical trial with Magacizumab, a humanized version of anti-LRG1 employed in this study, has been initiated for patients with neovascular age-related macular degeneration. Our preclinical data firmly support a crucial role of LRG1 in tumour metastasis and warrant further translational studies of LRG1 as a therapeutic target for metastasis.

References

1 Altorki, N. K. *et al.* The lung microenvironment: an important regulator of tumour growth and metastasis. *Nat Rev Cancer* **19**, 9-31, doi:10.1038/s41568-018-0081-9 (2019).

2 Steeg, P. S. Targeting metastasis. *Nat Rev Cancer* **16**, 201-218, doi:10.1038/nrc.2016.25 (2016).

3 Lambert, A. W., Pattabiraman, D. R. & Weinberg, R. A. Emerging biological principles of metastasis. *Cell* **168**, 670-691, doi:10.1016/j.cell.2016.11.037 (2017).

4 Augustin, H. G. & Koh, G. Y. Organotypic vasculature: From descriptive heterogeneity to functional pathophysiology. *Science* **357**, doi:10.1126/science.aal2379 (2017).

5 Butler, J. M., Kobayashi, H. & Rafii, S. Instructive role of the vascular niche in promoting tumour growth and tissue repair by angiocrine factors. *Nat Rev Cancer* **10**, 138-146, doi:10.1038/nrc2791 (2010).

6 Massague, J. & Obenauf, A. C. Metastatic colonization by circulating tumour cells. *Nature* **529**, 298-306, doi:10.1038/nature17038 (2016).

7 Cao, Z. *et al.* Molecular checkpoint decisions made by subverted vascular niche transform indolent tumor cells into chemoresistant cancer stem cells. *Cancer Cell* **31**, 110-126, doi:10.1016/j.ccell.2016.11.010 (2017).

8 Esposito, M. *et al.* Bone vascular niche E-selectin induces mesenchymal-epithelial transition and Wnt activation in cancer cells to promote bone metastasis. *Nat Cell Biol* **21**, 627-639, doi:10.1038/s41556-019-0309-2 (2019).

9 Hu, J. *et al.* Endothelial cell-derived angiopoietin-2 controls liver regeneration as a spatiotemporal rheostat. *Science* **343**, 416-419, doi:10.1126/science.1244880 (2014).

10 Lorenz, L. *et al.* Mechanosensing by beta1 integrin induces angiocrine signals for liver growth and survival. *Nature* **562**, 128-132, doi:10.1038/s41586-018-0522-3 (2018).

11 Srivastava, K. *et al.* Postsurgical adjuvant tumor therapy by combining anti-angiopoietin-2 and metronomic chemotherapy limits metastatic growth. *Cancer Cell* **26**, 880-895, doi:10.1016/j.ccell.2014.11.005 (2014).

12 Wieland, E. *et al.* Endothelial Notch1 activity facilitates metastasis. *Cancer Cell* **31**, 355-367, doi:10.1016/j.ccell.2017.01.007 (2017).

13 Gengenbacher, N., Singhal, M. & Augustin, H. G. Preclinical mouse solid tumour models: status quo, challenges and perspectives. *Nat Rev Cancer* **17**, 751-765, doi:10.1038/nrc.2017.92 (2017).

14 De Palma, M., Biziato, D. & Petrova, T. V. Microenvironmental regulation of tumour angiogenesis. *Nat Rev Cancer* **17**, 457-474, doi:10.1038/nrc.2017.51 (2017).

15 Peinado, H. *et al.* Pre-metastatic niches: organ-specific homes for metastases. *Nat Rev Cancer* **17**, 302-317, doi:10.1038/nrc.2017.6 (2017).

16 Wang, X. *et al.* LRG1 promotes angiogenesis by modulating endothelial TGF-beta signalling. *Nature* **499**, 306-311, doi:10.1038/nature12345 (2013).

17 Schlereth, K. *et al.* The transcriptomic and epigenetic map of vascular quiescence in the continuous lung endothelium. *Elife* **7**, doi:10.7554/eLife.34423 (2018).

18 Kano, A. *et al.* Endothelial cells require STAT3 for protection against endotoxin-induced inflammation. *J Exp Med* **198**, 1517-1525, doi:10.1084/jem.20030077 (2003).

19 Kim, K. J. *et al.* STAT3 activation in endothelial cells is important for tumor metastasis via increased cell adhesion molecule expression. *Oncogene* **36**, 5445-5459, doi:10.1038/onc.2017.148 (2017).

20 Yamamoto, M. *et al.* Overexpression of leucine-rich alpha2-glycoprotein-1 is a prognostic marker and enhances tumor migration in gastric cancer. *Cancer Sci* **108**, 2052-2060, doi:10.1111/cas.13329 (2017).

21 Shinozaki, E. *et al.* Serum leucine-rich alpha-2-glycoprotein-1 with fucosylated triantennary N-glycan: a novel colorectal cancer marker. *BMC Cancer* **18**, 406, doi:10.1186/s12885-018-4252-6 (2018).

22 Liu, Y. S. *et al.* Shotgun and targeted proteomics reveal that pre-surgery serum levels of LRG1, SAA, and C4BP may refine prognosis of resected squamous cell lung cancer. *J Mol Cell Biol* **4**, 344-347, doi:10.1093/jmcb/mjs050 (2012).

23 Furukawa, K. *et al.* Clinicopathological significance of Leucine-Rich alpha2-Glycoprotein-1 in sera of patients with pancreatic cancer. *Pancreas* **44**, 93-98, doi:10.1097/MPA.0000000000000205 (2015).

24 Andersen, J. D. *et al.* Leucine-rich alpha-2-glycoprotein-1 is upregulated in sera and tumors of ovarian cancer patients. *J Ovarian Res* **3**, 21, doi:10.1186/1757-2215-3-21 (2010).

25 Vanlandewijck, M. *et al.* A molecular atlas of cell types and zonation in the brain vasculature. *Nature* **554**, 475-480, doi:10.1038/nature25739 (2018).

26 Saito, K. *et al.* Gene expression profiling of mucosal addressin cell adhesion molecule-1+ high endothelial venule cells (HEV) and identification of a leucine-rich HEV glycoprotein as a HEV marker. *J Immunol* **168**, 1050-1059 (2002).

27 Murgai, M. *et al.* KLF4-dependent perivascular cell plasticity mediates pre-metastatic niche formation and metastasis. *Nat Med* **23**, 1176-1190, doi:10.1038/nm.4400 (2017).

28 Moss, S. E. *et al.* Preclinical development and testing of a therapeutic antibody against LRG1 [abstract]. In: Proc. Am. Assoc. Cancer Res. Ann. Meeting 2018; Cancer Res **78(13 Suppl)**, Abstract No. 5757 (2018).

29 Shojaei, F. *et al.* Tumor refractoriness to anti-VEGF treatment is mediated by CD11b+Gr1+ myeloid cells. *Nat Biotechnol* **25**, 911-920, doi:10.1038/nbt1323 (2007).

Acknowledgements: The authors would like to thank Prof. Dr. Jonathan Sleeman (ECAS, Medical Faculty Mannheim, Heidelberg University, Germany) for providing MMTV-PyMT tumours. We thank Prof. Dr. Ralf Adams (Max Planck Institute for Molecular Biomedicine, Muenster, Germany) for providing VECadCre^{ERT2} mice. We thank Prof. Dr. Franklin Constantini (Columbia University, New York, NY) for providing Rosa-YFP$^{fl/fl}$ (YFP$^{fl/fl}$) mice. We thank Prof. Dr. Mathias Heikenwälder (German Cancer Research Center, Heidelberg, Germany) for providing Stat3 $^{fl/fl}$ mice. We thank Ignacio Heras Murillo and Dr. Christopher Previti for technical assistance. We are most grateful for the excellent technical support of the Flow Cytometry, the Light Microscopy, the Genomics and Proteomics, the Omics IT and Data Management, and the Laboratory Animal Facilities of the DKFZ and IRCBC.

Funding: This work was supported by grants from the Deutsche Forschungsgemeinschaft (DFG) (project C5 within CRC1366 “Vascular control of organ function” [project number 39404578 to H.G.A.] and projects A2 and Z4 within CRC1324 “Wnt signalling” [project number 331351713 to H.G.A. and J.K.]); the European Research Council Advanced Grant “AngioMature” [project 787181 to H.G.A.]; and DFG-funded Research Training Group 2099 “Hallmarks of Skin Cancer” [project P8 to H.G.A.]. J.H. is supported by the “The Thousand Young Talents Recruitment Program”. J.G. and S.E.M. are supported by the Wellcome Trust Investigator Award [206413/B/17/Z] and Medical Research Council UK [MR/N006410/1].

Author contributions: MS, NG, AAAP, and HGA conceived and designed the study. MS, NG, AAAP, MK, LH, BK, BL, CM, JK, MSc, and JH performed experiments. DMK, SEM, and JG provided reagents. EB provided technical support. MS, NG, AAAP, and HGA analysed and interpreted data. MS and HGA supervised the project. MS, NG, AAAP, and HGA wrote the manuscript. All authors discussed the results and commented on the manuscript.

Competing interests: Authors declare no competing interests.

Data and materials availability: NGS data have been deposited in the Gene Expression Omnibus under accession numbers GSE131072 (bulk RNA-seq) and GSE131110 (single-cell RNA-seq). The mass spectrometry data files have been deposited to the ProteomeXchange Consortium under the accession number PXD013978.

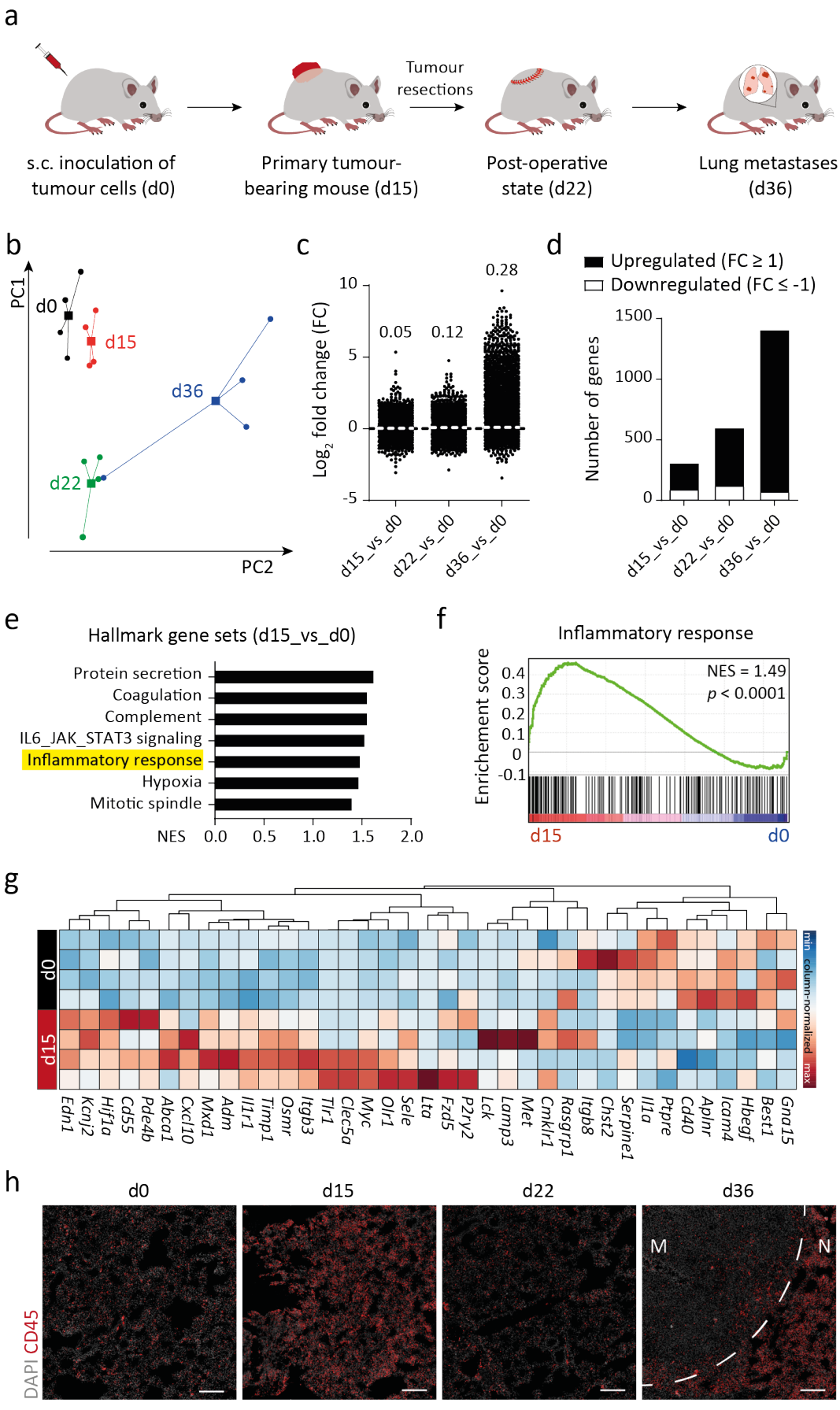
a
Tumour resections
s.c. inoculation of tumour cells (d0)
Primary tumour-bearing mouse (d15)
Post-operative state (d22)
Lung metastases (d36)
b
PC1
PC2
d0
d15
d22
d36
c
Log2 fold change (FC)
0.05
0.12
0.28
d15_vs_d0
d22_vs_d0
d36_vs_d0
d
Upregulated (FC ≥ 1)
Downregulated (FC ≤ -1)
Number of genes
e
Hallmark gene sets (d15_vs_d0)
Protein secretion
Coagulation
Complement
IL6_JAK_STAT3 signaling
Inflammatory response
Hypoxia
Mitotic spindle
NES
f
Inflammatory response
Enrichement score
NES = 1.49
p < 0.0001
d15
d0
g
d0
d15
min column-normalized max
Edn1 Kcnj2 Hif1a Cd55 Pde4b Abca1 Cxcl10 Mxd1 Adm Il1r1 Timp1 Osmr Itgb3 Tlr1 Clec5a Myc Olr1 Sele Lta Fzd5 P2ry2 Lck Lamp3 Met Cmklr1 Rasgrp1 Itgb8 Chst2 Serpine1 Il1a Ptpre Cd40 Aplnr Icam4 Hbegf Best1 Gna15
h
d0
d15
d22
d36
DAPI CD45
M
N

Fig. 1| Transcriptomic evolution of lung EC during metastasis. a, Schematic depiction of LLC spontaneous metastasis model, in which mice develop lung metastases following primary tumour resection. **b,** Principal component analysis of RNA-seq data of isolated lung EC (n = 4 samples for each time point). Circles and squares denote individual samples and centroid of each group, respectively. **c,** Dot plot showing Log_2 fold change (FC) for genes with RPKM ≥ 1 in at least one of the samples. The mean FC of all analysed genes is indicated for each comparison. **d,** Bar graph illustrating the number of significantly upregulated (↑) and downregulated (↓) genes in d15 (226 ↑, 89 ↓), d22 (480 ↑, 119 ↓), and d36 (1329 ↑, 71 ↓) lung EC as compared to d0. **e,** Gene Set Enrichment Analysis (GSEA) comparing d15 and d0 data sets. **f,** The inflammatory response gene set was found positively-correlated with d15 time point. **g,** Heatmap highlighting genes in the inflammatory response gene set. **h,** Immunofluorescence images showing infiltrating $CD45^+$ immune cells in the lung tissue. Scale bars = 200 µm. M = metastatic nodule; N = normal adjacent tissue; NES = normalized enrichment score.

339

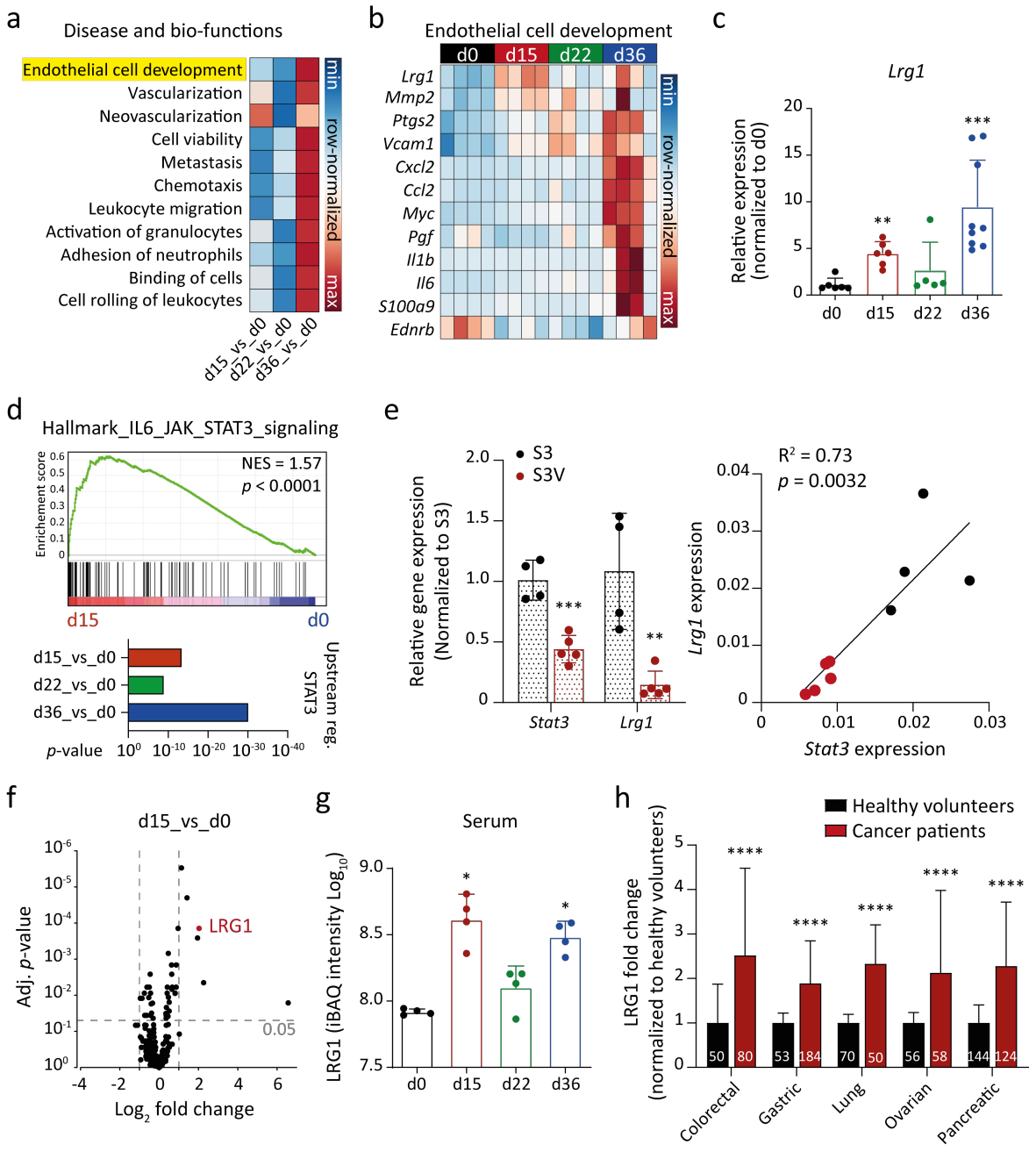
a
Disease and bio-functions
Endothelial cell development
Vascularization
Neovascularization
Cell viability
Metastasis
Chemotaxis
Leukocyte migration
Activation of granulocytes
Adhesion of neutrophils
Binding of cells
Cell rolling of leukocytes
min
row-normalized
max
d15_vs_d0
d22_vs_d0
d36_vs_d0
b
Endothelial cell development
d0
d15
d22
d36
Lrg1
Mmp2
Ptgs2
Vcam1
Cxcl2
Ccl2
Myc
Pgf
Il1b
Il6
S100a9
Ednrb
min
row-normalized
max
c
Lrg1
Relative expression (normalized to d0)
d0
d15
d22
d36
d
Hallmark_IL6_JAK_STAT3_signaling
Enrichement score
NES = 1.57
p < 0.0001
d15
d0
d15_vs_d0
d22_vs_d0
d36_vs_d0
Upstream reg. STAT3
p-value
e
S3
S3V
Relative gene expression (Normalized to S3)
Stat3
Lrg1
R² = 0.73
p = 0.0032
Lrg1 expression
Stat3 expression
f
d15_vs_d0
Adj. p-value
LRG1
0.05
Log2 fold change
g
Serum
LRG1 (iBAQ intensity Log10)
d0
d15
d22
d36
h
Healthy volunteers
Cancer patients
LRG1 fold change (normalized to healthy volunteers)
Colorectal
Gastric
Lung
Ovarian
Pancreatic

Fig. 2| LRG1 is systemically elevated during tumour progression. a, Comparison of disease and bio-functions was conducted using Ingenuity Pathway Analysis (IPA). Correlation scores (z-score) are shown for the selected disease and bio-functions. **b,** Genes involved in the EC development gene set are shown in row-normalized Log_2-expression values. **c,** qPCR quantitation of *Lrg1* expression in lung EC to validate RNA-seq data (mean ± SD, n = 5-9 mice). **, P<0.01; ***, P<0.001 (*two-tailed Mann-Whitney U test*). **d,** GSEA plot highlighting enriched IL6_JAK_STAT3 signalling on d15 as compared to d0 (upper panel). IPA analysis revealing STAT3 as an upstream regulator in disease stage-specific pattern. **e,** On the left, qPCR analysis of *Stat3* and *Lrg1* expression in lung EC isolated from tumour-bearing $Stat3^{fl/fl}$ (S3) or $Stat3^{fl/fl}$ X $VECadCre^{ERT2}$ (S3V) mice (mean ± SD, n = 4-5 mice). **, P<0.01; ***, P<0.001 (*multiple t-tests corrected with the Holm-Sidak method*). On the right, Pearson's correlation between *Stat3* and *Lrg1* expression. **f,** Volcano plot displaying FC and adjusted p-value for each identified protein in LC-MS analyses. The mean of 4 biological replicates is indicated. **g,** Shown are iBAQ intensities of LRG1 protein in serum samples (mean ± SD, n = 4 mice). *, P<0.05 (*two-tailed Mann-Whitney U test*). **h,** LRG1 protein amounts in sera of cancer patients and healthy volunteers were retrieved from previously-published articles (*13-17*). The bar graph shows relative LRG1 abundance normalized to the corresponding healthy cohort. Data normalization removes differences originating due to varying measurement techniques employed in different studies. The size of each sample cohort is indicated in the graph. ****, P<0.0001 (*multiple t-tests corrected with the Holm-Sidak method*).

340

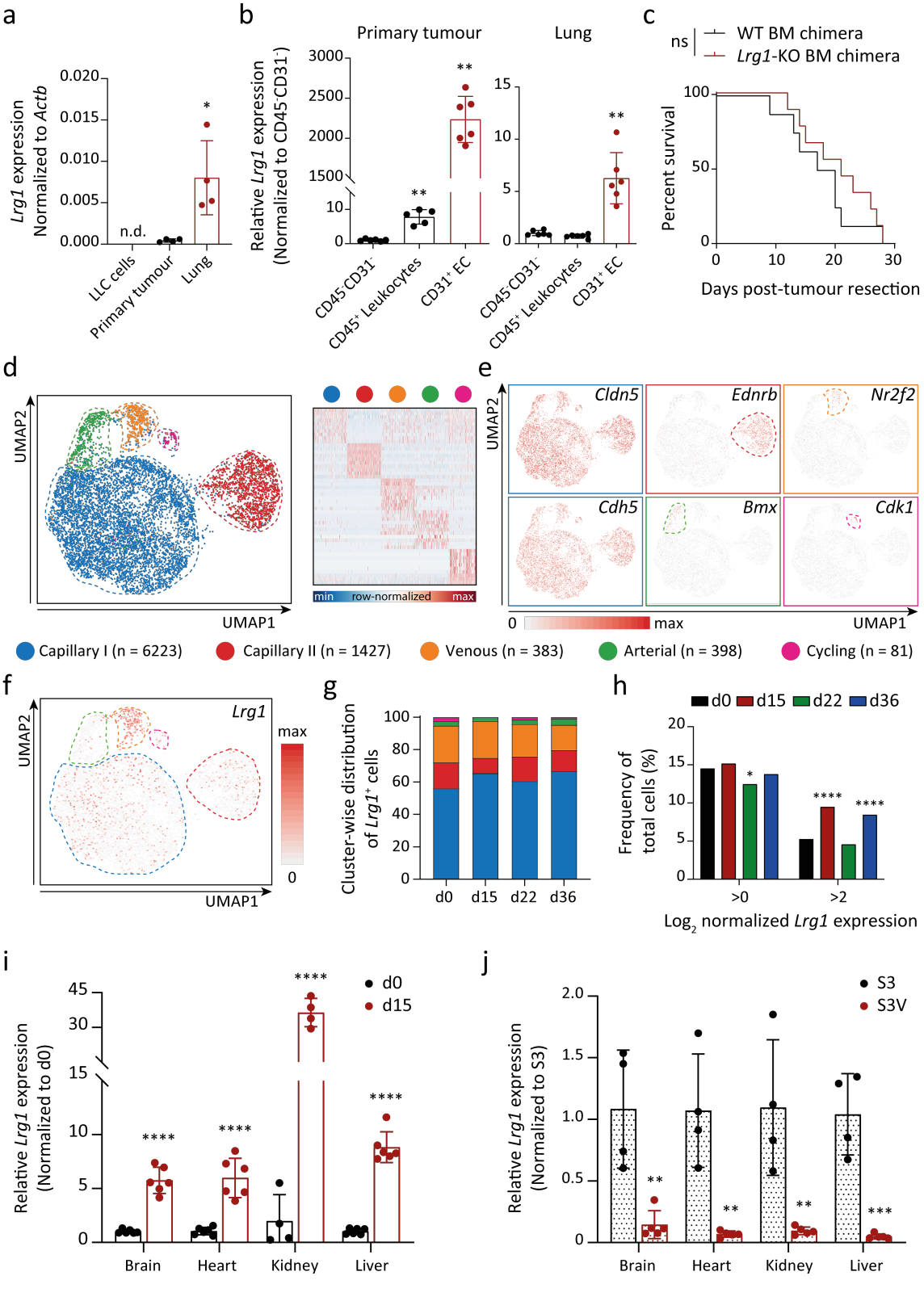
a
Lrg1 expression Normalized to Actb
n.d.
LLC cells
Primary tumour
Lung
b
Primary tumour
Lung
Relative Lrg1 expression (Normalized to CD45⁻CD31⁻)
CD45⁻CD31⁻
CD45⁺ Leukocytes
CD31⁺ EC
c
ns
WT BM chimera
Lrg1-KO BM chimera
Percent survival
Days post-tumour resection
d
UMAP2
UMAP1
min
row-normalized
max
e
Cldn5
Ednrb
Nr2f2
Cdh5
Bmx
Cdk1
Capillary I (n = 6223)
Capillary II (n = 1427)
Venous (n = 383)
Arterial (n = 398)
Cycling (n = 81)
f
Lrg1
g
Cluster-wise distribution of Lrg1⁺ cells
h
d0 d15 d22 d36
Frequency of total cells (%)
Log2 normalized Lrg1 expression
i
Relative Lrg1 expression (Normalized to d0)
Brain
Heart
Kidney
Liver
j
S3
S3V
Relative Lrg1 expression (Normalized to S3)

Fig. 3| Vascular endothelial cells are the major source of LRG1 and serve as a signal amplifier. a, Comparison of *Lrg1* expression between *in vitro*-cultured LLC cells, primary tumour and d15 lung tissue (mean ± SD, n = 4 mice). *, P<0.05 (*two-tailed Mann-Whitney U test*). **b,** EC, leukocytes, and $CD31^{-}CD45^{-}$ cells were isolated from primary tumours and d15 lung tissues. Dot plots show relative *Lrg1* expression in EC and leukocytes as compared to $CD31^{-}CD45^{-}$ cells (mean ± SD, n = 5-6 mice). **, P<0.01 (*two-tailed Mann-Whitney U test*). **c,** LLC tumours were implanted in WT or *Lrg1*-KO BM chimeras. Kaplan-Meier graph showing overall survival of mice after primary tumour resection (n = 8-9 mice). The comparison was rendered non-significant (ns) according to *Log-rank (Mantel-Cox) test*. **d,** On the left, UMAP visualization of colour-coded clusters of lung EC (n = 8,512 cells). On the right, gene signature of the capillary I/II, arterial, venous, and cycling subpopulations based on 10 most-upregulated genes. **e,** Feature plots indicating enriched genes for each identified subpopulation. EC-specific *Cldn5* and *Cdh5* were uniformly expressed by all subpopulations. **f,** Feature plot displaying *Lrg1* expression across all analysed lung EC. **g,** Shown is the cluster-wise spread of *Lrg1*-expressing cells for each sample. **h,** The graph highlights the frequency of *Lrg1*-expressing cells (Log_2-normalized expression >0 or >2) amongst the total number of cells per sample. *, P<0.05; ****, P<0.0001 (*two-sided Fischer's exact test*). **i,** *Lrg1* expression was analysed in EC isolated from multiple organs of d0 and d15 mice (mean ± SD, n = 4-6 mice). ****, P<0.0001 (*two-tailed Mann-Whitney U test*). **j,** *Lrg1* expression in multiorgan EC isolated from tumour-bearing $Stat3^{fl/fl}$ (S3) or $Stat3^{fl/fl}$ X $VECadCre^{ERT2}$ (S3V) mice (mean ± SD, n = 4-5 mice). **, P<0.01; ***, P<0.001 (*multiple t-tests corrected with the Holm-Sidak method*). n.d. = non-detectable.

341

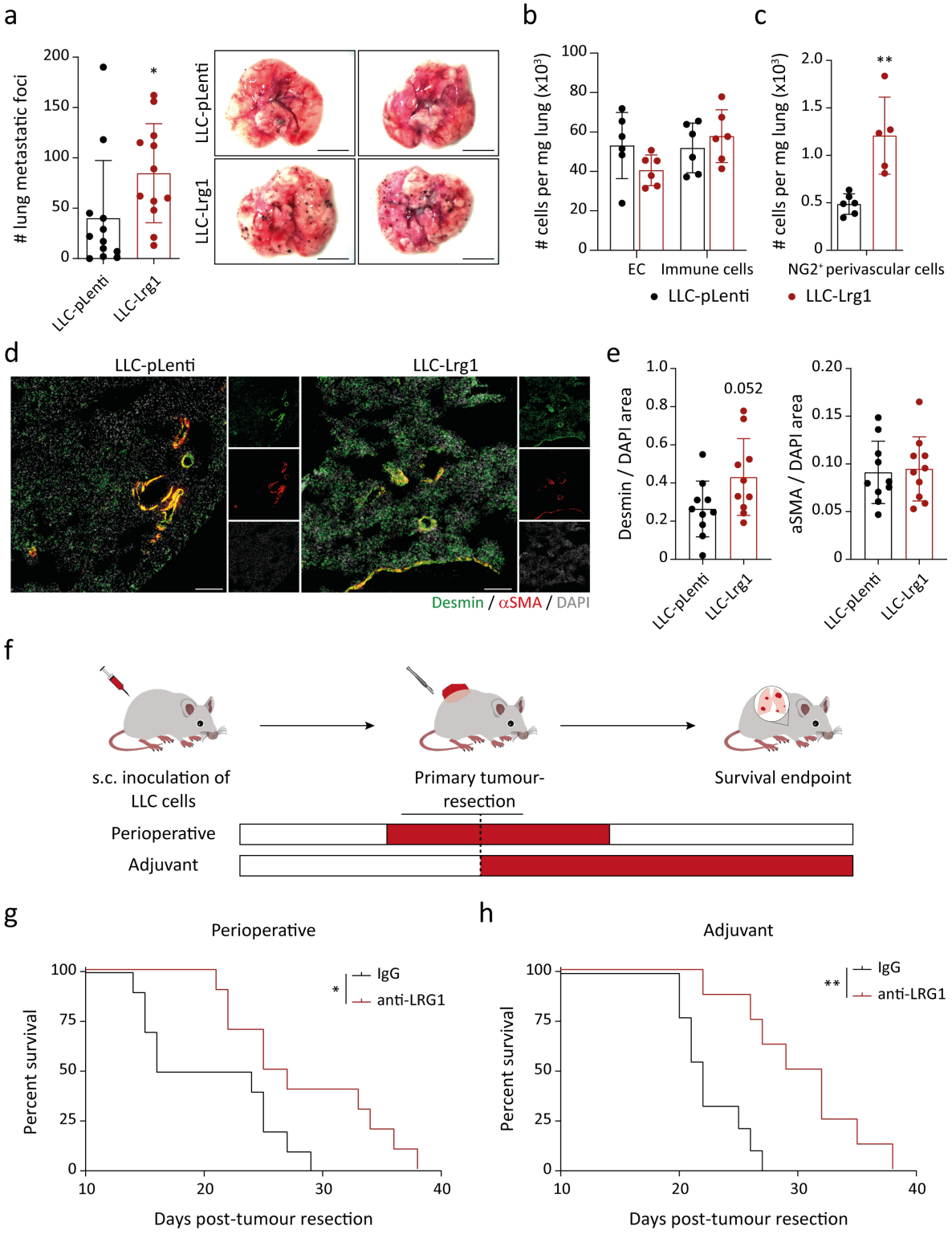
a
lung metastatic foci
LLC-pLenti
LLC-Lrg1
b
cells per mg lung (x10³)
EC
Immune cells
LLC-pLenti
LLC-Lrg1
c
cells per mg lung (x10³)
NG2⁺ perivascular cells
d
LLC-pLenti
LLC-Lrg1
Desmin / αSMA / DAPI
e
Desmin / DAPI area
0.052
aSMA / DAPI area
f
s.c. inoculation of LLC cells
Primary tumour-resection
Survival endpoint
Perioperative
Adjuvant
g
Perioperative
Percent survival
IgG
anti-LRG1
Days post-tumour resection
h
Adjuvant
Percent survival
IgG
anti-LRG1
Days post-tumour resection

Fig. 4| LRG1 neutralization inhibits metastasis. a, *Lrg1*-overexpressing LLC (LLC-Lrg1) or control-LLC (LLC-pLenti) cells were subcutaneously inoculated in mice. 7 days later, melanoma (B16F10) cells were intravenously injected. On the left, dot plot showing the number of melanoma metastases in the lung, and on the right, representative lung images (mean ± SD, n = 12 mice). Scale bars = 5 mm. *, P<0.05 (*two-tailed Mann-Whitney U test*). **b-e,** WT or NG2-Cre X $YFP^{fl/fl}$ mice were injected with either *Lrg1*-overexpressing LLC (LLC-Lrg1) or control-LLC (LLC-pLenti) cells. FACS-based quantitation of EC, immune cells, and $NG2^{+}$ perivascular cells in the lung of tumour-bearing mice **(b, c)** (mean ± SD, n = 5-6 mice). **, P<0.01 (*two-tailed Mann-Whitney U test*). Lung tissue sections were stained for Desmin (pericyte-specific) and αSMA (smooth muscle cell-specific). Representative images of lung sections **(d)**. Scale bars = 100 μm. Quantitation of Desmin/DAPI area and aSMA/DAPI area are shown **(e)** (mean ± SD, n = 10 mice; *two-tailed Mann-Whitney U test*). **f-h,** Therapeutic assessment of LRG1-blocking antibody 15C4 in LLC metastasis model using two different strategies **(f)**. Kaplan-Meier graphs showing overall survival of mice after primary tumour resection when treated with control-IgG or anti-LRG1 in perioperative (**g**; n = 10 mice) or postsurgical adjuvant (**h**; n = 8-9 mice) setting (50 mg/kg twice per week). *, P<0.05; **, P<0.01 (*Log-rank (Mantel-Cox) test*).

342